SI Appendix

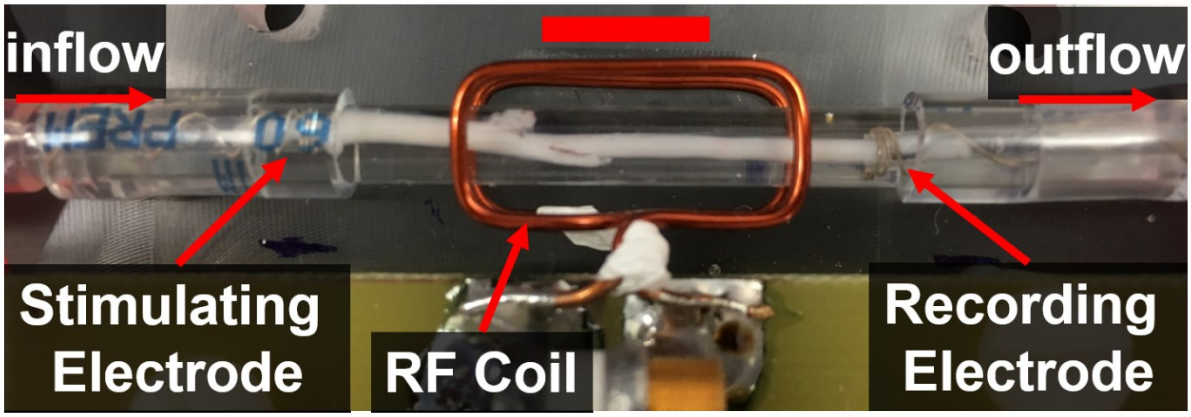

Figure S1. Close-up of the flow cell used for perfused nerve MRI studies with in-magnet electrophysiology recording. The nerve is held in place at the two ends by suction electrodes, one of which delivers electrical stimulation. The other suction electrode records the compound action potential (CAP) from the perfused nerve. The perfusion flow cell is shown with the single Helmholtz transmit/receive RF coil. Scale bar (top, center): 1 cm.

www.pnas.org/cgi/doi/10.1073/pnas.1801788115

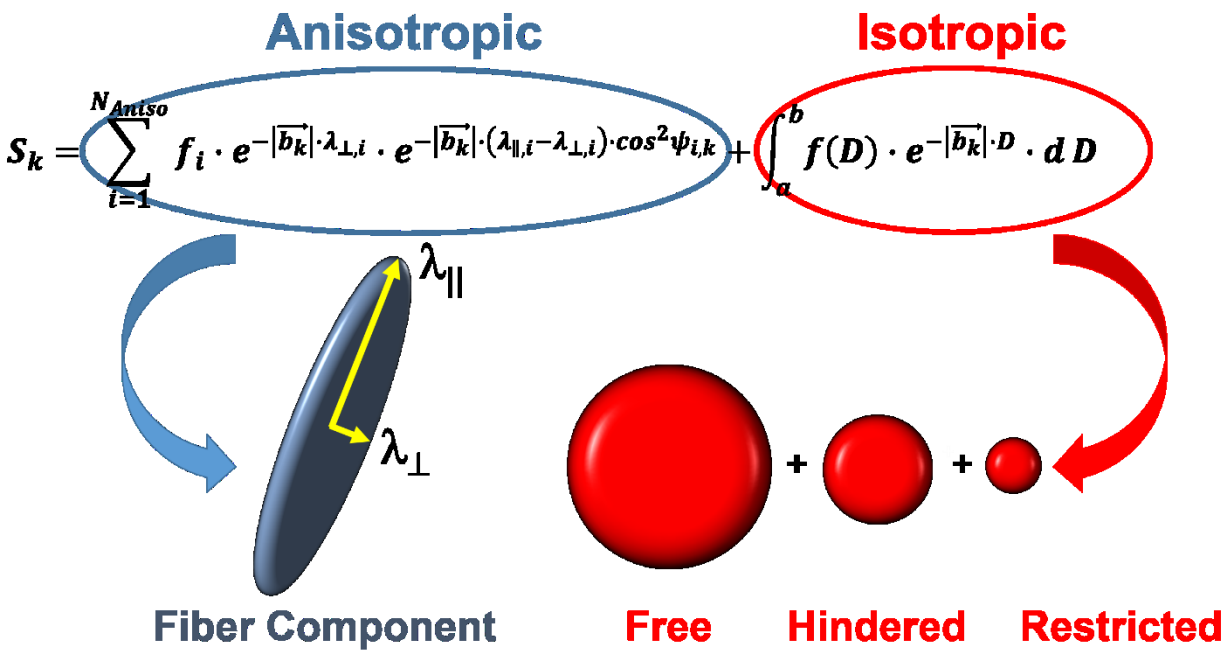

Figure S2. Pictorial Schematic of the Diffusion Basis Spectrum Imaging (DBSI) Signal Modeling. The diffusion-attenuated signal, measured along 25-directions and multiple diffusion-weightings (b values), is modeled as a sum of one or more anisotropic diffusion tensors and a spectrum of isotropic diffusivities (D). The overall diffusion signal can be decomposed into fiber fraction(s), and isotropic diffusion spectral components. In the current study, the restricted component (f_R) had $D \leq 0.3$ $\mu m^2/ms$, the hindered diffusion component (f_H) falls in the range, $0.3 < D < 2.0$ $\mu m^2/ms$, and the free diffusion component (f_{free}) accounts for $D \geq 2.0$ $\mu m^2/ms$.

Table S1. Icosahedral 25-direction diffusion gradient scheme.

Direction	Diffusion Gradient Scaling Factors Along Each Imaging Direction. $G_{i,diff} = d_i \cdot G_{max}$			b value (ms/μm²)*
	$d_{slice\text{-}select}$	$d_{phase\text{-}encode}$	$d_{readout}$	
1	0	-0.2	0	0.12
2	-0.17	-0.46	0	0.64
3	0.24	-0.62	0	1.24
4	0.21	-0.65	-0.42	1.78
5	-0.53	-0.53	-0.53	2.25
6	-0.16	-0.16	0.16	0.21
7	0.31	-0.31	0.31	0.81
8	0.11	-0.35	0.59	1.33
9	0	-0.29	-0.77	1.87
10	0	-0.33	0.88	2.41
11	0.15	-0.11	-0.29	0.35
12	-0.54	-0.17	0	0.82
13	0.69	-0.22	0	1.51
14	0.72	0	-0.45	2.06
15	-0.5	0	-0.82	2.47
16	-0.37	0	-0.14	0.40
17	-0.56	0	0.21	0.93
18	0.32	0.23	-0.64	1.57
19	-0.6	0.44	-0.46	2.02
20	0.67	0.49	0.52	2.71
21	0.07	0.22	0.38	0.56
22	-0.37	0.37	0.37	1.06
23	0.2	0.63	-0.41	1.67
24	-0.53	0.72	0	2.14
25	0.59	0.81	0	2.81

* Includes contributions of imaging gradients. G_{max} = 30.6 G/cm.

Supplementary Methods

Semi-automatic EM Image Segmentation

The Axon/Myelin/Vacuole segmentation is a region or pixel-based image segmentation method and involves the selection of initial seed points.

Pre-segmentation: The images are first pre-processed to enhance the contrast between the low intensity myelin and relatively higher intensity axonal regions, with default parameters of the built-in MATLAB (2015b) function, *imadjust*. In the second pre-processing step, images are filtered to smooth the intensities as well as sharpened boundaries/edges of the axon and myelin regions. Filtering is done in the frequency domain. Smoothing the intensities is implemented using a Gaussian low pass filter (~1.3% of the width of the Fourier transform of the image) and sharpening the edges with Gaussian high pass filter (~0.6% of the width of the Fourier transform of the image) as described in [http://www.cs.uregina.ca/Links/class-info/425/Lab5/index.html]. This is seen to improve segmentation and demarcates their edges from surrounding regions.

Region growing segmentation: This approach examines neighboring pixels of initial seed points and determines whether the pixel neighbors should be added to the region based on pixel intensity. The region growing segmentation is based on MATLAB (2015b) built-in function *grayconnected,* which finds connected regions of similar intensity in the grayscale image, within a range of intensity values determined by a threshold or tolerance that can be user controlled. The user specifies the intensity value to use as a starting point, the seed pixel, and the function *grayconnected* generates a binary mask image, where all of the foreground pixels are 8-connected to the seed pixel by pixels of similar intensity.

Post-segmentation: The area of the mask (segmented region corresponding to axon, vacuole or myelin area) is measured using the MATLAB (2015b) built-in function *regionprops.* The diameter of this region is also obtained from this area using the formula for area of an equivalent circle, $A = (\pi/4)D^2$, where A = area of segmented region, D = equivalent diameter of segmented region. The measurements (area and diameter) for each axon and myelin segmented are recorded or saved into a table/spreadsheet (.csv format). Areas are reported in pixel units.

The user places a seed pixel marker in myelin, axon, and possibly vacuole regions (depending upon whether or not they are seen in a given image). In practice, the segmented areas of vacuole overlap with axon. The myelin area reported in the .csv output is the total area bounded by the myelin, including the enclosed axon and vacuole roi's. Conversion from image pixels to areas in μm^2 are done offline based upon the known magnification/scale of the acquired EM image.

Supplementary Results

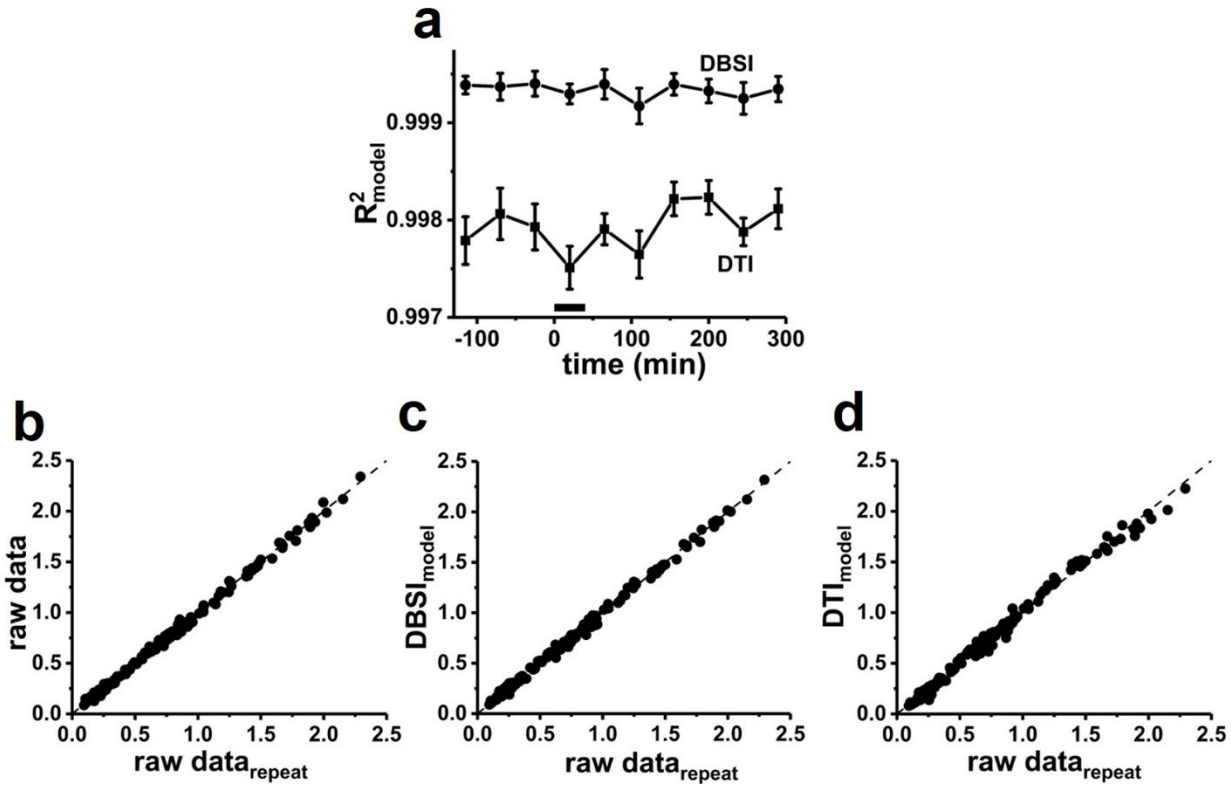

Figure S3. Goodness of Fit (R^2) and Cross-Validation Comparison of DBSI and DTI Model Fits. For a 3 × 3 voxel ROI in the center of the nerve, the R^2 for fitting of data vs. model across the time-series for the six nerves undergoing 40 min x 100 Hz stimulation are shown in panel **A.** Symbols used are closed circles (R^2 for DBSI model) and closed squares (R^2 for DTI model). The timing of applied stimulus is indicated by the horizontal black bar. Panel **B** shows R^2 for repeat measurements. Signal intensities (in scanner signal intensity units) of each of the 25 different diffusion weightings/directions are shown for each of the six nerves. For each data point, the x coordinate corresponds to the intensity measured in the second baseline (pre-stimulus) MRI measurement and the y coordinate corresponds to the intensity measured in the subsequent repeat pre-stimulus baseline measurement. The line of identity (y = x) is plotted as a dashed line. Reproducibility in repeat measurements is very high due to high SNR and absence of bulk physiological motion. Panel **C** plots data from the cross-validation assessment of the DBSI model in each ROI. Across the individual trials (pairs of repeat measurements), the ability of the DBSI model to predict the second, repeat measurement dataset was comparable to measurement reproducibility ($R^2_{CV,DBSI}$ = 0.99926 ± 0.00044, mean ± SD, n = 6, vs. R^2_{repeat} = 0.99933 ± 0.00009). The line of identity is shown as a dashed line. Panel **D**: Analogous CV data are shown for the DTI ($R^2_{CV,DTI}$ = 0.9978 ± 0.0007, mean ± SD, n = 6).

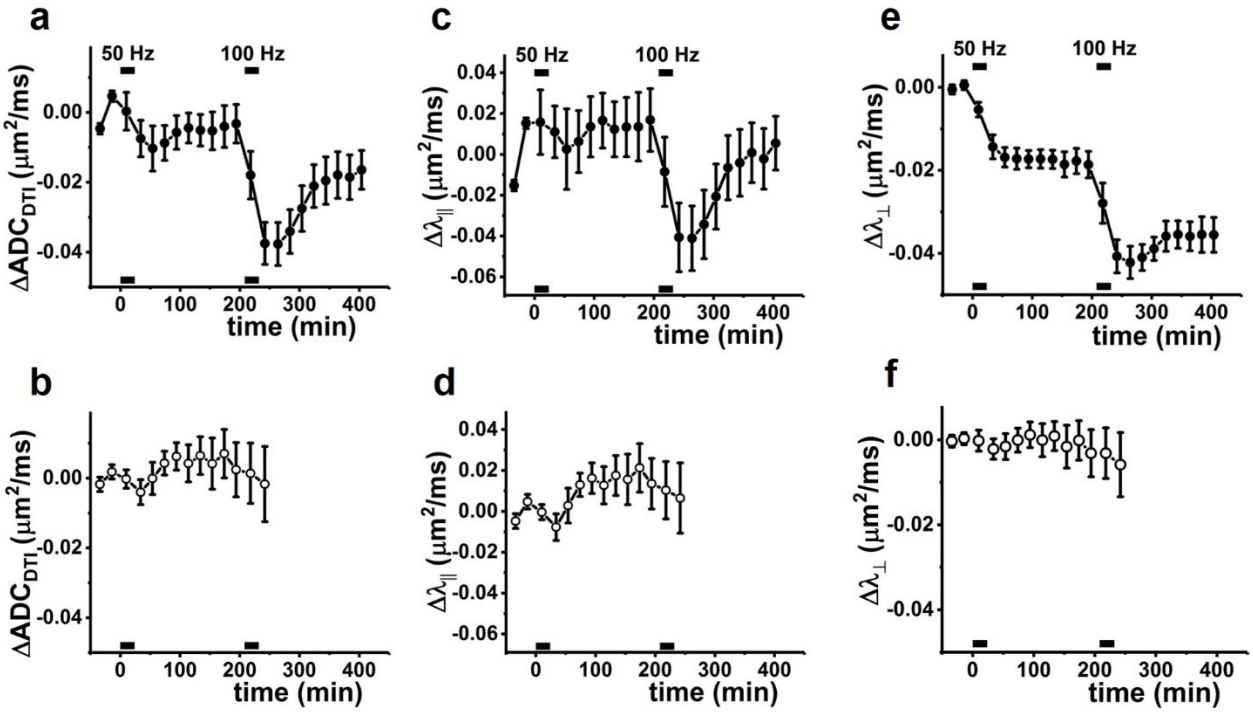

Figure S4. Frog sciatic nerve diffusion fMRI time-course from DTI modeling. Results derived from image data acquired with a 32 × 32 image matrix (20-minute temporal resolution). The top row of panels (**A,C,E**) depict DTI-model parameter results for perfused nerves (n = 6, mean ± sem) that underwent two rounds of electrical stimulation (24 minutes × 50 Hz and 24 minutes × 100 Hz) separated by a 3-hour recovery period. For comparison, the bottom row of panels (**B,D,F**) depict results for nerves (n = 3, mean ± sem) that underwent perfusion-only (no electrical stimulation) in a shorter time-course—ending at the time-point corresponding to the second post-stimulus time-point. Periods of electrical stimulation are depicted by the black bars in the top row. For reference, the corresponding times are also indicated in the bottom, perfusion-only, row of figures. Of the DTI parameters, the diffusion fMRI $\Delta\lambda_{\perp}$ appears to show the most stability (smaller error bars/data scatter).

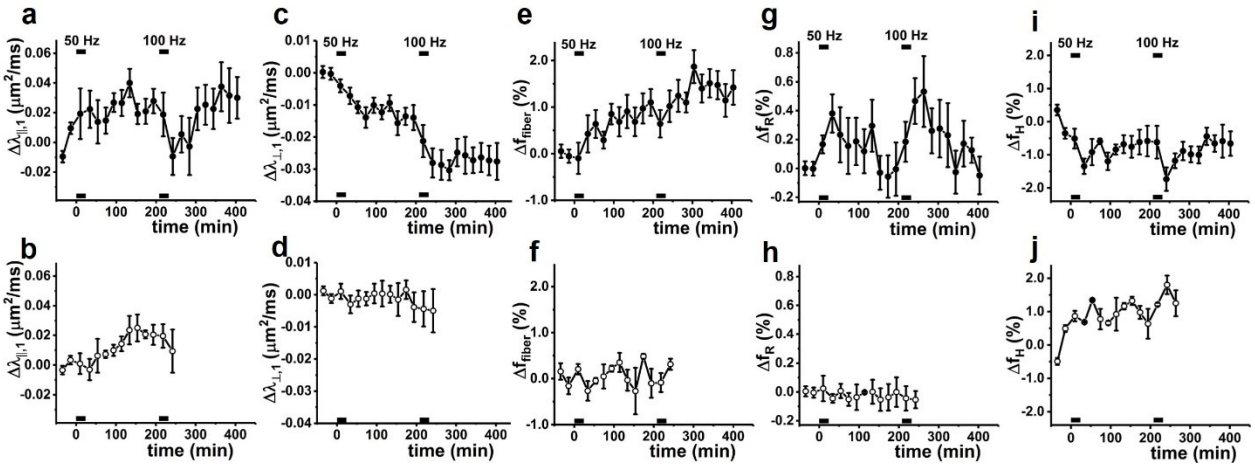

Figure S5. Frog sciatic nerve diffusion fMRI time-course from DBSI modeling. Results derived from image data acquired with a 32 × 32 image matrix (20-minute temporal resolution). The top row of panels (**A,C,E,G,I**) depict DBSI-model parameter results for perfused nerves (n = 6, mean ± sem) that underwent two rounds of electrical stimulation (24 minutes × 50 Hz and 24 minutes × 100 Hz) separated by a 3-hour recovery period. For comparison, the bottom row of panels (**B,D,F,H,J**) depict results for nerves (n = 3, mean ± sem) that underwent perfusion-only (no electrical stimulation) in a shorter time-course—ending at the time-point corresponding to the second post-stimulus time-point of the top row. Periods of electrical stimulation are depicted by the black bars in the top row. For reference, the corresponding times are also indicated in the bottom, perfusion-only, row of figures. Panel **E** and **F** suggests some that electrical stimulation produces swelling of the DBSI fiber fraction. Comparing panels **G** and **H**, the stimulation-induced transient increase in restricted fraction is still observable, albeit with more scatter than in **Figure 2C**. Panels **I** and **J** show changes in DBSI hindered fraction.

Table S2. Comparison of Diffusion Metrics Derived from Diffusion Imaging Data Acquired With Different Spatial Resolutions.

		Comparison for Perfusion-only Nerves (n = 3)	
		64 × 64 (mean ± sem)	**32 × 32** (mean ± sem)
DTI Parameters	$\mathbf{ADC_{DTI}}$ ($\mu m^2/ms$)	0.822 ± 0.007	0.851 ± 0.009
	$\lambda_{\parallel}$ ($\mu m^2/ms$)	1.562 ± 0.015	1.600 ± 0.021
	$\lambda_{\perp}$ ($\mu m^2/ms$)	0.451 ± 0.003	0.476 ± 0.005
DBSI Parameters	$\lambda_{\parallel,1}$ ($\mu m^2/ms$)	1.59 ± 0.02	1.61 ± 0.03
	$\lambda_{\perp,1}$ ($\mu m^2/ms$)	0.362 ± 0.009	0.365 ± 0.012
	$\mathbf{f_{fiber}}$ (%)	79 ± 2	76 ± 2
	$\mathbf{f_R}$ (%)	0.44 ± 0.04	0.22 ± 0.05